High velocity resolution observations of OH main line masers in the M82 starburst

M.K. Argo¹, A. Pedlar², R.J. Beswick², T.W.B. Muxlow², D.M. Fenech³

1. Curtin Institute of Radio Astronomy, Curtin University of Technology, Bentley, Perth, WA 6845, Australia

- 2. University of Manchester, Jodrell Bank Observatory, Macclesfield, Cheshire SK11 9DL, UK
- 3. Department of Physics and Astronomy, University College London, Gower Street, London WC1E 6BT, UK

29 May 2022

ABSTRACT

Using the VLA, a series of high velocity resolution observations have been made of the M82 starburst at 1.6 GHz. These observations follow up on previous studies of the main line OH maser emission in the central kiloparsec of this starburst region, but with far greater velocity resolution, showing significant velocity structure in some of the maser spots for the first time. A total of thirteen masers were detected, including all but one of the previously known sources. While some of these masers are still unresolved in velocity, these new results clearly show velocity structure in spectra from several of the maser regions. Position-velocity plots show good agreement with the distribution of H_I including interesting velocity structure on the blue-ward feature in the west of the starburst which traces the velocity distribution seen in the ionised gas.

Key words: masers - galaxies: individual: M82 - galaxies: ISM - galaxies: starburst

INTRODUCTION

Masers are common in star forming regions within the Milky Way and many nearby galaxies are now known to contain masers of one flavour or another, with powerful megamasers detected out to greater and greater redshifts (e.g. the recent discovery of a water maser at a redshift of 2.639; Impellizzeri et al. 2008). Maser sources require dense molecular gas and a nearby source of energy to create the required population inversion. The presence of one or more type of maser in a given region can therefore be used to probe the physical conditions of the gas, making them useful tools for understanding complex starburst systems.

Galactic OH masers located in star forming regions are typically very compact ($\sim 10^{13}$ cm), have very narrow line widths ($\sim 1 \,\mathrm{km \, s^{-1}}$) and flux ratios (1667/1665) less than one. In contrast, megamaser emission in ULIRGs tends to be spatially unresolved, have line widths >100 km s⁻¹, flux ratios >1 and total intensities typically a factor of 10^6 greater that that of Galactic sources (Lo 2005). In between these classes lie the so-called "kilomasers" with luminosities around 10³ timer greater than typical Galactic sources. These are found in nearby starbursts where the star formation rate is intermediate between that of the Milky Way and those of distant ULIRGs.

The nearby starburst M82 is the prototypical starburst and one of the most intensively studied. It is known to contain large amounts of gas (e.g. HI, Wills et al. 2000; CO, Shen & Lo 1995), have strong outflows (e.g. winds traced

by $H\alpha$, Shopbell & Bland-Hawthorn 1998), numerous supernova remnants and HII regions (e.g. Muxlow et al. 1994; McDonald et al. 2002; Fenech et al. 2008) and a history of strong star formation due to a past encounter with M81, although there is evidence that the rate of star formation has decreased significantly in the last 5 Myr (Beirão et al. 2008).

Various types of maser have been detected in the central starburst of M82 over the last few decades, as would be expected for a galaxy with a significant molecular gas content and strong continuum emission, and these features can be used to investigate the molecular gas conditions and dynamics within the galaxy. Main line OH masers were first detected in M82 by Weliachew et al. (1984) and, while they are significantly stronger than maser emission seen in the Milky Way, they are fainter than the megamasers seen at the other extreme in AGN.

Previous studies of the OH masers in M82 (Argo et al. 2007) have found 10 individual masing regions, none of which are spatially resolved with the 1".4 beam of the VLA. These observations, however, were designed to probe the OH absorption in M82, rather than the masers, so the spectral resolution was comparatively poor.

This paper describes follow-up observations carried out with the VLA in 2006 at higher spectral resolution in order to investigate the maser population in more detail. Unless otherwise stated, all positions are given in J2000 coordinates in the format aa".aaa bb.bb corresponding to 09^h55^maa.aaa and +69°40'bb" bb respectively. At the distance of M82

ObsID	Date	Time (LST)		
AA302a	Feb 7/8	0200 - 1030		
AA302b	Feb 16/17	0230 - 1030		
AA302c	Feb 21	0300 - 0900		
AA302d	Mar 19	0330 - 0930		
AA302e	Mar 27/28	0430 - 1230		

Table 1. VLA observations carried out in 2006 during programme AA302. The structure of each observation was similar and included scans on flux and bandpass calibrators as well as scans on M82 and 0954+745 at two frequencies designed to cover the required bandwidth.

(3.6 Mpc, Freedman et al. 1994), one arcsecond corresponds to a linear distance of 17.5 parsecs.

2 OBSERVATIONS

High velocity resolution observations were carried out using the VLA in A configuration during February and March 2006. These observations were intended to to enable the detection of masers with narrow velocity widths which were not bright enough to be detectable in the much wider channels of the 2002 observations, and attempt to resolve velocity structure in those already known.

The experiment was carried out in five separate runs, details of which are given in Table 1. The sources 1331+305, 0319+415 and 0954+745 were used as flux, bandpass and phase calibrators respectively. The observations each consisted of scans on the flux and bandpass calibrators as well as scans on M82 and 0954+745 at two frequencies such that the total frequency coverage was sufficient to cover the entire velocity range expected across M82 at both 1665 and 1667 MHz with some overlap between IFs at the band edges. To achieve this, the correlator was used in 4-IF mode with a bandwidth of 1.5 MHz and 128 channels per IF, resulting in a velocity resolution of $2 \, \mathrm{km \, s^{-1}}$. Velocities in this paper are quoted relative to $225 \, \mathrm{km \, s^{-1}}$, the systemic radio LSR velocity of M82.

The data from each run were edited and calibrated separately before being combined prior to imaging. For each run, the process was as described below. Firstly, the channel zero file (created by averaging the inner 75 per cent of the band) was examined for each source, polarization, IF and frequency in order to detect major problems such as dead antennas and bad scans. This pseudo-continuum dataset was then calibrated using standard methods for continuum calibration with the VLA. Each of the four IFs were calibrated separately. Together with the flag table, the final calibration tables from this step, one for each IF, were then copied over to the corresponding line datasets. A bandpass calibration was then performed for each frequency using 0319+415 before the data were split out separately for each IF. The datasets for each of the epochs were then combined to create one dataset per IF from which image cubes were made. Each of the four cubes were then inspected separately using various tasks within AIPS.

When the first run, AA302a, was initially examined in the AIPS task POSSM, a large amount of interference was discovered. The data were examined more closely in the visual task SPFLG and strong interference was found to be present on all sources, varying both in time and with baseline. It is not telescope specific, nor is it apparent on all baselines at a given time. It is generally stronger at 1665 MHz than in the 1667 MHz data and both stronger and more prevalent in Stokes RR than LL, but largely it does only affect a small subset of the channels. A patient examination of each source in each frequency, stokes and IF was made in SPFLG for each run and data were flagged on all sources, polarisations, IFs and times where the problem was seen to appear. Several checks were made throughout this process to ensure that all interference was removed.

The resulting calibrated cubes, one for each of the four IFs, were imaged and then continuum subtracted using a set of line free channels at either end of the band before being examined for maser features. The mean 3σ noise in each cube was $2.7\,\mathrm{mJy\,beam^{-1}\,channel^{-1}}$ (similar sensitivity to the low velocity resolution MERLIN data from 1995 but a factor of almost six worse than the 2002 VLA observations due to the much narrower channels). By comparing measurements of continuum sources in M82 it was found that, to within the uncertainties, the positions and flux scales matched in all four final datasets.

3 RESULTS AND GENERAL COMMENTS

Table 2 lists all the maser features in this dataset which were present at 5σ or more in more than one channel at either one or both frequencies, together with their positions, peak fluxes or limits in each line, flux ratio between the two lines and the velocity at the peak of the line profile. Figure 1 shows the maser locations across the central kpc of the M82 starburst. This figure was constructed from the four final continuum-subtracted image cubes: each cube was collapsed in frequency, ignoring the five channels at either end of the band in each cube, and the resulting images were then summed to create one image. The diagram shows all of the maser features above 5σ in more than one consecutive channel, whether they are detected at $1665\,\mathrm{MHz}$, $1667\,\mathrm{MHz}$ or both.

Despite the lower sensitivity per channel than in the VLA 2002 dataset, all but one of the previously known masers appear in this dataset. Due to the narrower channels used in these observations, the masers generally appear much brighter here than in the 2002 dataset. The exception to this is 50.02+45.8, a maser which has remained undetected since MERLIN observations in 1995 (see Section 5).

In general, fluxes measured in this dataset are more than a factor of two brighter than those measured in the much broader channels used in the 2002 observations. The smallest difference is 50.95+45.4 where the difference is a factor of 1.9 at $1667\,\mathrm{MHz}$ (2.78 at $1665\,\mathrm{MHz}$), and the largest is 53.11+47.9 which is brighter at $1665\,\mathrm{MHz}$ by a factor of >10 in 2006. This feature is narrow even at a velocity resolution of $2\,\mathrm{km\,s^{-1}}$ so could be brighter still.

Positions measured in the 2006 data are all within half a beam of those measured in 2002 at the same spatial resolution (1".4). The mean positional offset between sources in the two epochs is 0".17 with 51.94+48.3 having the largest offset (0".36).

Spectra from each maser feature are shown in Figure 2 ($1665\,\mathrm{MHz}$) and Figure 3 ($1667\,\mathrm{MHz}$). Most of the maser

J2000 ID	R.A. (J2000)	Dec. (J2000)	S ₁₆₆₅ (mJy)	S ₁₆₆₇ (mJy)	Ratio (1667:1665)	$_{(\mathrm{km}\mathrm{s}^{-1})}^{\mathrm{Velocity}}$
53.64+50.1	53°.643	50'.'11	11.4	15.0	1.32	115
53.11 + 47.9	53.113	47.88	20.2	< 2.7	< 0.13	47
52.73 + 45.8	52.729	45.77	16.9	< 2.7	< 0.16	3
52.42 + 49.2	52.416	49.18	11.1	< 2.7	< 0.24	62
51.94 + 48.3	51.937	48.29	11.5	< 2.7	< 0.23	-7
51.55 + 48.5	51.543	48.47	< 2.7	7.42	> 2.75	-27
51.27 + 44.3	51.276	44.29	13.2	32.4	2.44	-113
50.95 + 45.4	50.950	45.35	29.1	34.4	1.18	-133
50.54 + 45.5	50.542	45.50	5.15	< 2.7	< 0.52	-34
50.38 + 44.3	50.381	44.24	22.8	116	5.09	-151
50.07 + 43.1	50.066	43.06	< 2.7	7.66	> 2.84	-158
49.71 + 44.2	49.714	44.21	< 2.7	12.1	>4.48	-83
48.43 + 41.9	48.432	41.96	6.18	19.0	3.07	-125

Table 2. Definite maser detections identified from the VLA 2006 data. Limits on the measured peak flux densities are given as 3σ . Velocities are quoted relative to the systemic velocity of $225\,\mathrm{km\,s^{-1}}$. Where a line was present in both frequencies, the measured velocities were the same in both frequencies. The maser IDs here are constructed from the J2000 positions measured in this dataset (relative to $09^{\mathrm{h}55^{\mathrm{m}}} + 69^{\circ}40'$) and are used throughout this paper. Maser IDs in bold are those which are new in these observations. Uncertainties on fluxes are $\pm 2.7\,\mathrm{mJy}$, and $\pm 1.1\,\mathrm{km\,s^{-1}}$ on velocities.

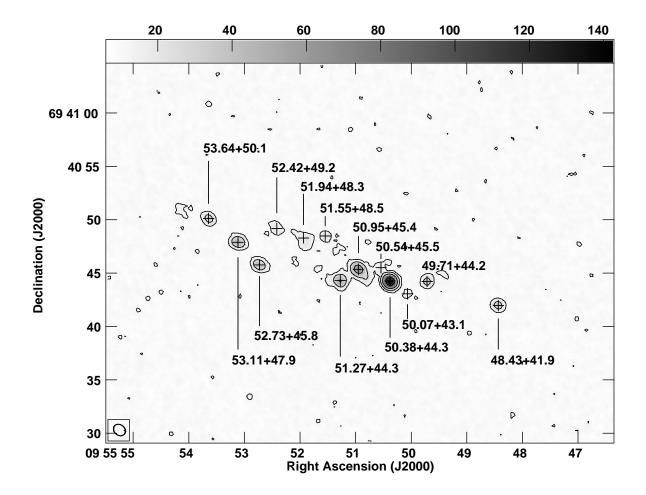


Figure 1. All masers detected in the VLA 2006 observations at $>5\sigma$. The image is a combination of both frequencies showing masers at both 1665 and 1667 MHz. The contours are $(-1,1,2,4,8,16,32) \times 3 \,\text{mJy/beam}$ and the labels correspond to the maser IDs given in Table 2.

4 M.K. Argo et al.

features have only one narrow peak, but a subset are broader with a shoulder on one side or the other. The spectra are discussed further in Section 5.

Although these observations were not ideal for detecting absorption, some is present in the data, mainly to the east of the dynamical centre. The deepest absorption features are coincident with those found in previous HI studies at the eastern end of the central kpc.

4 NOTES ON INDIVIDUAL SOURCES

Brief notes are given here for each maser comparing with the results given in Argo et al. (2007). More detailed discussion of the properties of the population are given in the following section. Note that the features are identified by their J2000 position in this dataset with labels corresponding to those in column one of Table 2. Where a maser was detected in 2002, the velocities measured here are the same to within the uncertainties, with the exception of 51.94+48.3 (see below). Unless otherwise noted, SNRs and HII regions are given by their B1950 positions as reported by McDonald et al. (2002), H₂O masers are from Baudry & Brouillet (1996) and OH satellite line features are from Seaquist et al. (1997).

Note that all masers detected in the 2002 data are also detected here. The only previous maser which is undetected here is 50.02+45.8 which was only detected in the MERLIN 1995 observations.

- (i) 53.64+50.1 is still detected in both lines but with a slightly larger line ratio than in 2002. The measured velocity is the same (within the errors) for both lines and matches that measured in $2002~(122\pm9\,\mathrm{km\,s^{-1}})$. It lies within a beam of the HII region 44.93+63.9~(B1950~position; McDonald et al. 2002).
- (ii) 53.11+47.9 is again only present at $1665\,\mathrm{MHz}$ where its velocity $(46.7\pm1.1\,\mathrm{km\,s^{-1}})$ is consistent with that measured in $2002\,(56\pm9\,\mathrm{km\,s^{-1}})$. It is apparently coincident with the supernova remnant 44.43+61.9.
- (iii) 52.73+45.8 is also only present at $1665\,\mathrm{MHz}$, as in 2002, and the measured velocity is within the uncertainty of the previous result $(8\pm9\,\mathrm{km\,s^{-1}})$. This source is co-located with a supernova remnant (44.01+59.6) and a satellite line feature (F4; Seaquist et al. 1997) which is seen in absorption at $1720\,\mathrm{MHz}$ and strongly in emission at $1612\,\mathrm{MHz}$ with a velocity of $8\pm4\,\mathrm{km\,s^{-1}}$, consistent with the velocity measured here. While listed as a supernova remnant by McDonald et al, the behaviour in the satellite lines led Seaquist et al to suggest the source as an AGN candidate, and EVN observations by Wills et al. (1999) show comparable structure and brightness to SgrA. It is also within 1.11 of an X-ray point source (CXOM82 J095552.8+694047; Griffiths et al. 2000), but the main line ratio is atypical of megamaser sources associated with AGNs (Lonsdale 2002).
- (iv) 52.42+49.2 is a new maser in this dataset. It is only present at $1665\,\mathrm{MHz}$ and is apparently coincident with a possible water maser detection (43.7+62.75) from Baudry & Brouillet (1996), listed as a possible feature only due to not being $>5\sigma$ in more than one channel. Interestingly, the authors note that this feature has an anomalous velocity compared to the molecular emission along the same line of sight. The velocity measured for the OH feature 52.42+49.2 in the 2006 data is $+62.1\,\mathrm{km\,s^{-1}}$ while

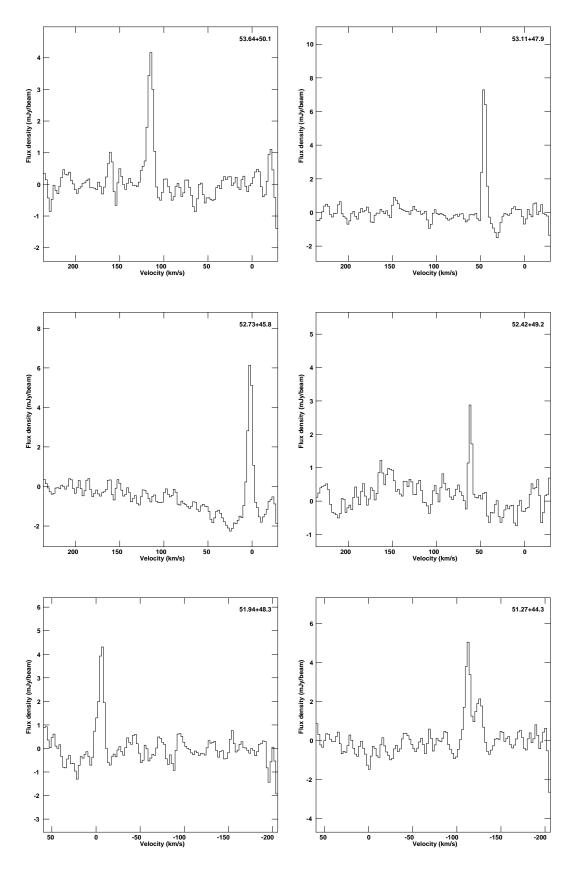


Figure 2. Spectra of each maser listed in Table 2 at 1665 MHz, arranged in order of decreasing R.A. Each maser is seen in two or more adjacent channels with a flux greater than five times the rms noise level. The data have been continuum subtracted and are smoothed with a Gaussian of width 2 channels. The x-axis velocity scale is calculated relative to the rest frequency of the 1665 MHz line. Continued

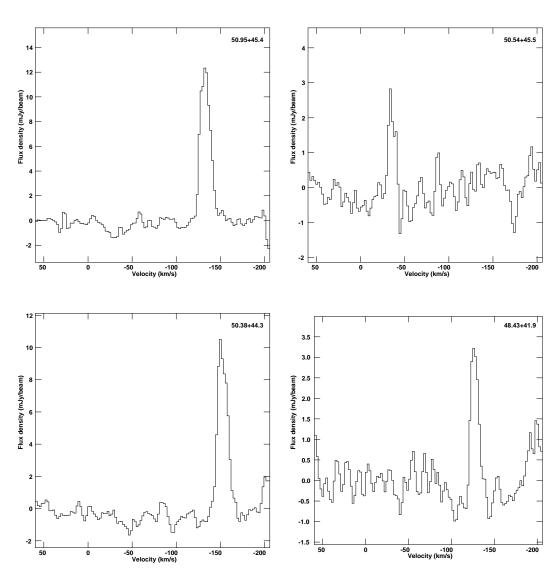


Figure 2: continued.

the H_20 feature of Baudry & Brouillet is at a velocity of $-64.6 \,\mathrm{km \, s^{-1}}$, putting it well off the main distribution and away from any other features on the eastern side of the galaxy on the p-v diagram (see Section 5.4).

- (v) 51.94+48.3 has the largest position offset compared to previous detections of all the masers discussed here, although the offset (0″.36) is smaller than the size of the beam (1″.4). It was the weakest detection at 1665 MHz in 2002 and not detected at all at 1667 MHz. In 2006 it is also only detected at 1665 MHz but with a slightly different velocity at it's peak (2002: $12\pm 9\,\rm km\,s^{-1}$; 2006: $-7.3\pm 1.1\,\rm km\,s^{-1}$). The detection in 2002 was only definite at 1665 MHz¹ where it is superimposed on an absorption feature and hence was only just above the detection threshold. The 2006 detection is much more significant. It is along the same line of sight (within the size of the beam) as the continuum source 43.21+61.3 (B1950) from Rodriguez-Rico et al. (2004) detected at 8.3 and 43 GHz and classified as a possible HII region.
- (vi) 51.55+48.5 is a new maser in this dataset. It is only present at 1667 MHz where it is the weakest detection in this line and has no apparent associations with known continuum sources or other maser features.
- (vii) 51.27+44.3 is detected in both lines as it was in 2002. The measured position and velocity matches within the uncertainties (2002: $-106\pm9\,\mathrm{km\,s^{-1}}$; 2006: $-113\pm2\,\mathrm{km\,s^{-1}}$) but the line ratio has increased by a factor of two since 2002. It is within a VLA beam of both a significant (S1) and a possible H₂O maser (42.5+59.25) from Baudry & Brouillet (1996), within an arcsecond of an HII region (42.48+58.4) and within a beam of two others.
- (viii) 50.95+45.4 is once again also detected in both lines. It is the only feature where the line ratio has decreased between the two epochs, but the velocities are the same within the uncertainties. It is apparently coincident with both an HII region (42.21+59.2) and an H₂O maser (S2).
- (ix) 50.54+45.5 was brighter at 1665 MHz in 2002 but was detected in both lines. In the 2006 observations however, it is only detected (weakly) at 1665 MHz. It has no known associations with other masers or continuum features.
- (x) 50.38 + 44.3 is apparently coincident with a known HII region (41.61+57.9) and a water maser (S3). It is again the brightest OH maser feature detected in M82 and continues to have the most extreme line ratio.
- (xi) 50.07 + 43.1 is a new feature in this dataset and is only detected at 1667 MHz. It is not coincident with any known continuum feature, or any other maser detection, and its velocity is consistent with it being located on the blue ward arc (see Section 6.4).
- (xii) 49.71 + 44.2 is again only significantly detected at 1667 MHz. This feature is within a beamwidth of two HII regions (40.95+58.8; 40.96+57.9) and is also coincident with a possible H₂O feature (40.9+58.25). At the same position there is a weak feature (3.7 mJy) at 1665 MHz with a velocity ($-79.8 \,\mathrm{km\,s^{-1}}$) slightly offset from that measured at 1667 MHz ($-83.0 \,\mathrm{km\,s^{-1}}$). However, as it is $<5\sigma$, this 1665 MHz feature is not included in further discussions.

(xiii) 48.43 + 1.9 is again detected in both lines and is brighter at $1667 \,\mathrm{MHz}$ with a velocity comparable to that measured in previous datasets. It is within a beamwidth of an H_{II} region (39.68+55.6) and an H₂O maser detection (S4).

5 DISCUSSION

Of the 13 features seen in these observations, ten have been identified in previous work (Argo et al. 2007). Five masers are seen in both lines, a further five are seen only at 1665 MHz and three are present only in the 1667 MHz data. The only maser reported previously which has not been detected again here is 50.02+45.8, a source which was only detected in low-velocity resolution MERLIN observations carried out in 1995 and, although it was detected at $>3\sigma$ in 1995, it was the weakest detection in that dataset and has not been detected subsequently.

This section discusses apparent associations, spatial structure, line ratios, spectra, velocity distribution and the blue ward arc in more detail.

5.1 Possible associations

Of the five masers visible only at $1665\,\mathrm{MHz}$, two are apparently coincident with supernova remnants (53.11+47.9; 52.73+45.8), one of which is also co-located with a satellite line feature (52.73+45.8), one lies within a beam of a possible $\mathrm{H_2O}$ feature (52.42+49.2), and two have no apparent associations (51.94+48.3; 50.54+45.5). Of the three sources seen only at $1667\,\mathrm{MHz}$, two are new detections (51.55+48.5; 50.07+43.1) neither of which appear associated with known continuum features or other maser detections. The third of these, 49.71+44.2, was previously noted to coincide with an HII region. The five features visible in both lines (53.64+50.1; 51.27+44.3; 50.95+45.4; 50.38+44.3; 48.43+41.9) are all apparently coincident with known HII regions.

As has been noted previously, considering that the disk of M82 is viewed almost edge on these apparent associations are likely to be due to line of sight effects. These observations lack the required spatial resolution to determine whether the sources are physically related.

5.2 Spatial structure

 $^{^1\,}$ Figure 4 of Argo et al. (2007) shows the incorrect spectrum for this maser (labelled 51.87+48.3).

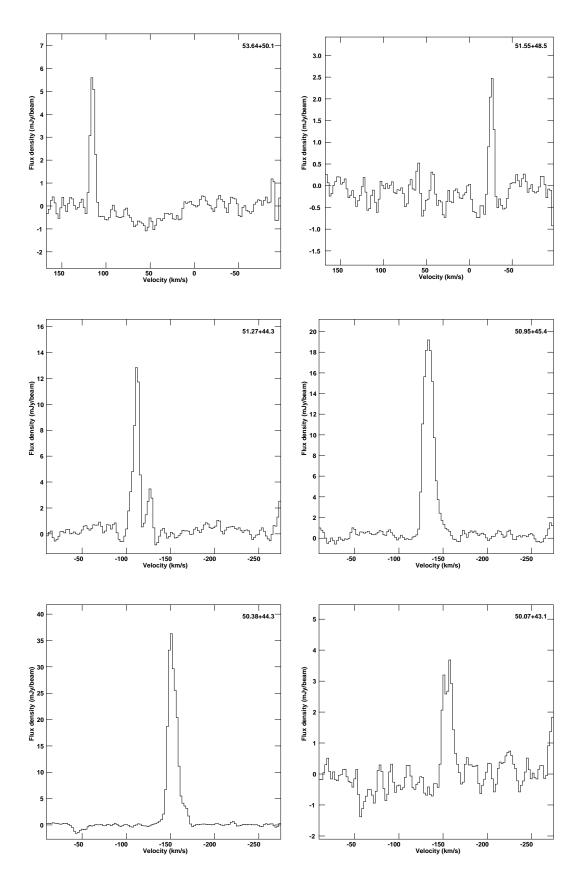


Figure 3. Spectra of each maser listed in Table 2 at 1667 MHz, arranged in order of decreasing R.A. Each maser is seen in two or more adjacent channels with a flux greater than five times the rms noise level. The data have been continuum subtracted and are smoothed with a Gaussian of width 2 channels. The x-axis velocity scale is calculated relative to the rest frequency of the 1667 MHz line. Continued

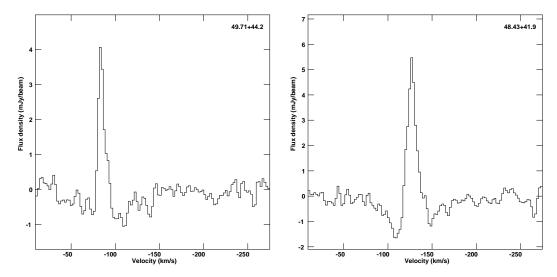


Figure 3: continued.

As with the 2002 VLA data, the resolution of these observations is insufficient to see spatial structure in the maser regions. This is not surprising given that the physical size of typical Galactic masers placed at the distance of M82 would be much smaller than the linear resolution of the VLA at that distance (22 pc at $1.6\,\mathrm{GHz}$).

The only maser which shows convincing physical extension is 50.95+45.4 near the centre of the galaxy. Previous VLA observations also showed a similar extension to the SW which was best fitted by three Gaussians. Higher resolution observations with MERLIN showed a weak second component along the same position angle (Argo et al. 2007). These observations show an extension in the same direction (Fig. 1) which varies in frequency: the position of the peak moves from NE to SW as frequency increases. The same effect can be seen in both main lines and can also be seen clearly in the p-v diagram (see Section 5.4). It is likely that the extension of 50.95+45.4 is due to several maser spots lying fairly close together but with different velocities, the resolution of the VLA at this frequency is not sufficient to distinguish them.

In the 1667 MHz data, 51.27+44.3 appears to be slightly extended to the east. Again, due to the small size of known Galactic maser regions, this is likely caused by the superposition in space of two unresolved maser spots, rather than any intrinsic structure. This is also illustrated by features 50.54+45.5 and 50.38+44.3 which are located very close together on the sky, but are clearly separate features as their velocities are -34 and $-151\,\mathrm{km\,s^{-1}}$ respectively.

5.3 Line ratios

For an optically thin cloud in local thermal equilibrium, the expected ratio for emission from the 1665 and 1667 MHz lines is 1.8. Column 7 of Table 2 shows line ratios of each feature present in this dataset. Where a feature is only detected in one line, the limit is calculated from the 3σ noise in the other line. Note that, compared to typical velocity resolutions used in observations of Galactic masers, these

observations are still under-resolving the masers in M82, so it is possible that they could be brighter still.

In 2002, six features were detected in both lines allowing line ratios to be calculated. One of these features, 50.54+45.5, had a line ratio of 0.69 in 2002 but is not detected above 5σ at 1667 MHz in 2006. The other five masers in this group were all detected above 5σ in more than two channels in the 2006 observations in both lines. Of these, three have line ratios which are consistent with those measured in 2002, given a typical 5 per cent flux uncertainty on each measurement. However, 51.27+44.3 and 48.43+41.9 both have ratios significantly larger than those measured in the 2002 data. In the case of 51.27+44.3 the ratio in 2006 is twice that measured in 2002.

As in 2002, 49.71+44.2 is again only detected at 1667 MHz. Two of the three new maser features (51.55+48.5 and 50.07+43.1) are also only present in the 1667 MHz dataset and so have limits calculated from the 3σ noise measured in the 1665 MHz line. 53.11+47.9, 52.73+45.8 and 51.94+48.3 are again only seen at 1665 MHz in this dataset. 50.54+45.5 was previously detected at $>5\sigma$ in both lines in 2002 where it was stronger at 1665 MHz, but in the 2006 data it is only visible at 1665 MHz.

With the exception of 50.95+45.4, for all masers which are detected in both lines the ratios have increased since the 2002 observations. The greatest difference is for 51.27+44.3 which has doubled from a ratio of 1.2 in 2002 to 2.4 in 2006. The feature 50.38+44.3 continues to have the most extreme line ratio, 4.7 in 2002, 5.1 in 2006. Interestingly, while it is a significant distance from the dynamical centre of M82 and apparently coincident with an HII region, 50.38+44.3 has a high line ratio more typical of megamasers associated with AGN than Galactic masers in regions of star formation (Lonsdale 2002).

One caveat with comparing measured line ratios between data sets is that whether or not the line is resolved affects the measured peak flux. In some cases, the lines are clearly resolved in frequency, whereas with previous measurements they were unresolved.

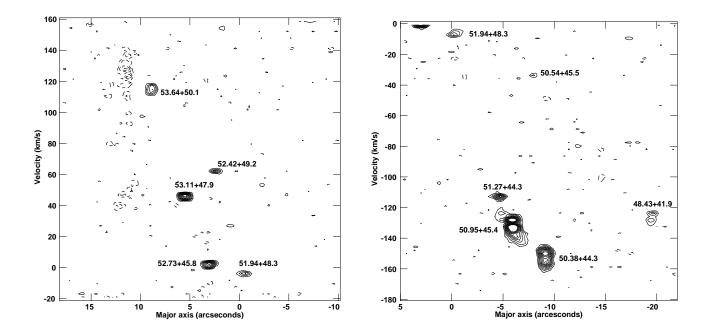


Figure 4. Position-velocity plots for each IF in the $1665\,\mathrm{MHz}$ dataset. Features are labelled according to their positions as listed in Table 2. Contours are $(-10\ \mathrm{to}\ 10)\times 1.6\ \mathrm{mJy/bm}$. The velocity $0\ \mathrm{km\,s^{-1}}$ represents the systemic velocity of M82 ($225\ \mathrm{km\,s^{-1}}$) and the centre of M82 is taken to be $09^{\mathrm{h}}55^{\mathrm{m}}52^{\mathrm{s}}.132 + 69^{\circ}40'46''.14$ (J2000).

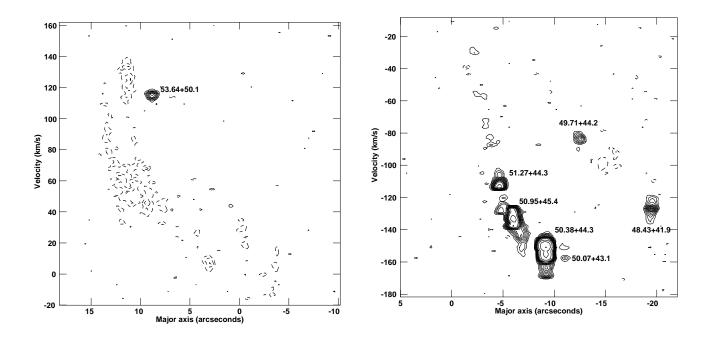


Figure 5. Position-velocity plots for each IF in the 1667 MHz dataset. Features are labelled according to their positions as listed in Table 2. Contours are $(-10 \text{ to } 10) \times 1.6 \text{ mJy/bm}$ (left) and $(-10 \text{ to } 10, \text{ then } 12, 16, 24, 40, 68) \times 1.6 \text{ mJy/bm}$ (right).

5.4 Spectra and velocity structure

Figures 2 and 3 show the spectra of each feature $>5\sigma$ in more than one consecutive channel at 1665 and 1667 MHz respectively. The spectra are arranged in order of decreasing R.A. (left to right in Figure 1) and labelled according to their IDs in Table 2. The p-v plots in Figures 4 and 5 show the distribution of masers in velocity along the major axis of the galaxy. Following the method of Wills et al. (2000), before producing the p-v plots each cube was first rotated 17° anticlockwise so that the major axis of the galaxy was horizontal. Then each cube was compressed to one plane along the declination axis, ignoring the five channels at either end of the band where the response was poor.

The velocity distribution of the masers in this dataset lies along the same distribution as that seen in the CO and H_I distributions in Wills et al. (2000). As seen in the 2002 observations however, several masers lie along an arc blue ward of the main distribution. As with the H_I gas, the strongest features of this arc lie on the same axis as that of the ionised [Ne II] gas distribution of Achtermann & Lacy (1995). The cause of this feature has been suggested to be either an expanding superbubble or the x_2 orbits of an inner bar (Wills et al. 2000).

The spectra of the two brightest masers, 50.95+45.4 and 50.38.44.3, both show a blue wing at $1667\,\mathrm{MHz}$ which is less obvious at $1665\,\mathrm{MHz}$. It can be seen from the right-hand panels of Figures 4 and 5 that this region of the p-v diagram has some interesting structure. Both 50.95+45.4 and 50.38+44.3 show velocity structure with significant extension in both lines, structure which is more extended at $1667\,\mathrm{MHz}$ than it is at $1665\,\mathrm{MHz}$. This can be seen more clearly in Figure 6 where the two p-v plots are superimposed for this region. The redward extension of 51.27+44.3 and the low-level bluest third peak of 50.38+44.3 are only visible at $1667\,\mathrm{MHz}$, while 50.95+45.4 has broadly the same structure in both lines with extensions to both the east (red) and west (blue) and a double-peaked structure, with the extension again greatest at $1667\,\mathrm{MHz}$.

Another maser which shows velocity structure is 50.07+43.1 which appears to have two narrow peaks, but is only present at $1667\,\mathrm{MHz}$. The two peaks here are more closely spaced in frequency than those of 51.27+44.3 and have similar brightnesses, with the bluer peak marginally stronger.

In the p-v diagram, the feature 51.27+44.3 also clearly has two peaks at 1667 MHz with the bluer peak significantly stronger. The p-v plots in Figures 4 and 5 show that there is also emission at the same position on the major axis but with an even bluer velocity, blending into the large feature at 50.95+45.4. This illustrates the complexity of the ISM in M82. The second, weaker peak in the spectrum of 51.27+44.3 in Figures 2 and 3 is actually this weak feature close to 50.95+45.4. Given the linear resolution of the VLA, it is likely that this feature is a different maser spot, physically unconnected but along the same line of sight as 51.27+44.3, with a velocity similar to that of 50.95+45.4.

The structure of this group of masers in the p-v diagram suggests several closely spaced maser regions sited along the blue ward arc, and it is likely that this region contains many clouds at different velocities spread out over a significant volume. This region is discussed further in Section 6.4.

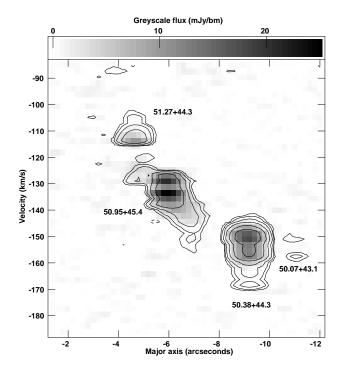


Figure 6. The region around 50.95+45.4 in more detail. The $1665\,\mathrm{MHz}$ data is shown as greyscale with a range from 0 to $25\,\mathrm{mJy/bm}$, while the $1667\,\mathrm{MHz}$ data is plotted as contours of $(-1,1,2,4,8,16,32)\times1.9\,\mathrm{mJy/bm}$. The emission at $1667\,\mathrm{MHz}$ is noticeably broader in frequency than that at $1665\,\mathrm{MHz}$.

The only source located in the main velocity distribution to show significant velocity structure is 48.43+41.9 which is weak but has a double-peaked profile in the p-v plot at 1665 MHz, but a stronger single peak with pronounced wings at 1667 MHz.

6 COMPARISON WITH OTHER WAVELENGTHS

Due to its proximity, M82 has been well studied across the electromagnetic spectrum. It is interesting to compare the emission seen here in OH with features seen at other wavelengths in order to gain a greater understanding of the conditions and dynamics within the central kiloparsec of the galaxy.

6.1 Stars and dust

Figure 7 shows the positions of the masers plotted on an archival image from the ACS instrument on the HST using a 680-980 nm filter. While it should be noted that there are a lack of directly comparable features between the optical and radio fields, the astrometry of the HST image was tweaked using positions of objects in the field from the 2MASS and SDSS catalogues, with a resulting estimated rms positional uncertainty of 0.% (the symbols are 1 arcsecond in diameter). Different symbols indicate whether the maser is detected at just $1665\,\mathrm{MHz}$, just $1667\,\mathrm{MHz}$, or both. As this

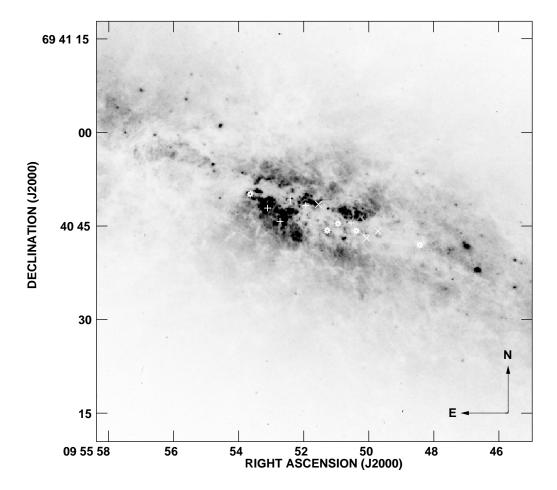


Figure 7. The OH masers in M82 plotted over the optical emission from the central starburst. Grey scale: $H\alpha$ HST ACS image (program ID 9788, PI Ho). The positions of the masers are also plotted. Those visible at just 1665 MHz are shown as plusses, those detected only at 1667 MHz as crosses, and those present in both lines as stars.

figure shows, and as might be expected from maser emission associated with star formation regions, most of the masers are located within dusty, heavily obscured regions of the central starburst, particularly the masers located on the blue ward arc.

6.2 Atomic and molecular gas

To carry out a comparison with the absorption seen in the atomic gas traced by HI absorption, 1420 MHz data from the VLA archive has been used from an A-array observation on November 27th 1996 (programme AW444; Wills et al. 2000). The dataset was reduced using standard spectral line procedures in AIPS and a p-v plot was produced using the same method as described in Section 5.4. While the spatial resolution of the two datasets is similar, the 1996 observation was carried out with a bandwidth of 3.125 MHz over 63 channels resulting in a velocity resolution of 10.3 km s⁻¹. To compare this with the higher velocity resolution OH data from 2006, the two IFs at each frequency in the OH observations were combined using the AIPS task UJOIN resulting in two datasets of 190 channels each, one for each of the OH lines.

The HI data has only 63 channels so to compare the datasets the number of channels was artificially increased using the AIPS task XSMTH which can interpolate over channels. The resulting p-v plots are shown in Figure 8.

The deep absorption in the OH data is coincident with the deepest absorption features seen in the HI data at the eastern end of the disk. The masers appear to avoid the deepest HI absorption features, but this could be due to OH absorption being present at the same locations since strong absorption can hide weak maser peaks (as illustrated by the 2002 VLA data).

The maser features on the blue arc are coincident with the arc seen in the HI data on the blue ward side of the 'hole' (Wills et al. 2000) also seen in the CO (Shen & Lo 1995) and [Ne II] (Achtermann & Lacy 1995). This feature is discussed further in Section 6.4. More recently, Seaquist et al. (2006) mapped M82 in ¹²CO J=6-5 and found evidence for the same blue feature, and a corresponding weak feature to the east of the galaxy, as well as higher than average excitation in the region surrounding 41.95+57.5 where the bright masers on this feature are located.

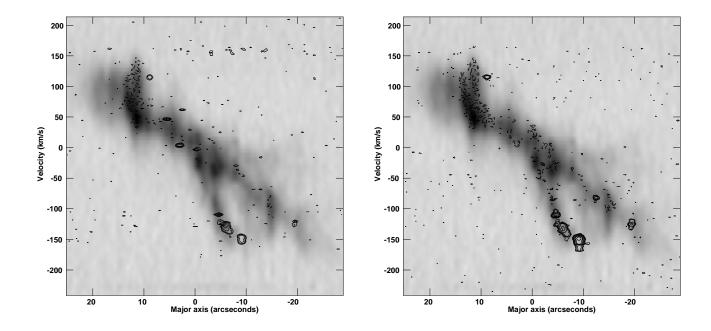


Figure 8. A comparison between the OH and HI datasets. The 1665 MHz p-v plot is on the left, 1667 MHz on the right. The greyscale shows the HI absorption while the contours show the OH absorption and emission. The greyscale range is from 0 to -28 mJy/bm, while contours are drawn at $(-4, -2, -1, 1, 2, 4, 8, 16, 32, 64) \times 2.4$ mJy/bm (left) and 1.5 mJy/bm (right). The centre of M82 is taken to be $09^{h}55m52^{h}132 + 69^{\circ}40^{\circ}46^{\prime\prime}14$ (J2000) and the velocity has been corrected for a systemic velocity of $225 \,\mathrm{km \, s^{-1}}$.

6.3 Ionised gas

Comparing the positions of the masers with the [NeII] emission from Achtermann & Lacy (1995), several masers appear around the edge of the $12.8\mu\mathrm{m}$ ring. The three bright features around the location of the radio continuum source 41.95+57.5 also appear to coincide with the [NeII] peak labelled W1. This is not surprising given that their velocity distribution also coincides with that of the [NeII], rather than with the main disk rotation; the velocity distribution of the [NeII] emission is much steeper than that of the main disk traced by the HI or OH absorption and the western side of this steeper distribution is well traced by the brighter masers in this dataset.

Figure 9 shows the positions of the masers relative to the ionised gas as traced by 408 MHz radio emission from a MERLIN observation in 1994 (Wills et al. 1997). From this figure it can be seen that the masers tend to avoid the peaks of low frequency emission and, in particular, several of the masers are located within the 'hole' feature noted by Wills et al. This feature is $\sim 100 \,\mathrm{pc}$ in diameter, roughly centered on the compact object 41.95+57.5, and has been suggested to be due to free-free absorption by gas in a giant HII region ionised by a large stellar cluster (note that this is also the location of the high excitation seen in ¹²CO J=6-5 transition by Seaguist et al. 2006 mentioned above). The masers located in this region however are not typical of Galactic masers found in star forming regions as they all (except 50.54+45.5) have line ratios >1. Interestingly, it is also this group which are located on the blue feature in the p-v diagram except (again) 50.54+45.5 which has a velocity which places on the main distribution.

6.4 The blue arc

As has already been noted, an obvious feature of the p-v plots is the arc to the west of the disk which lies blue ward of the main distribution. It has been shown previously that the OH absorption traces the arc well, and that several of the brightest maser features in M82 are located on the arc (Argo et al. 2007). Wills et al. (2000) compare the distribution of HI traced by absorption with that of CO emission and ionised [NeII] finding a similar feature in both HI and CO, and noted that the steeper gradient of the [NeII] gas matches at least the eastern edge of this feature in the HI and CO distributions. This information was used to model a bar feature in the centre of M82. Matsushita et al. (2005) showed a p-v plot of $^{12}CO(1-0)$ together with H41 α and noted that the known OH and H₂O masers were mainly clustered in velocity around the "superbubble". This arc is also present in recent optical data of emission lines over the central kpc of the disk (Westmoguette et al. 2009).

The gradient of the main distribution measured from these data is found to be $\sim 6\,\mathrm{km\,s^{-1}\,arcsec^{-1}}$, in agreement with $\sim 6.5\,\mathrm{km\,s^{-1}\,from}$ HI and CO measurements of Wills et al. (2000), whereas the gradient of the emission on the eastern edge of the blue ward arc is $\sim 20\,\mathrm{km\,s^{-1}\,arcsec^{-1}}$, similar to that of the [NeII] gas distribution. The three brightest masers at 1667 MHz are all located on this feature while the fainter features are on the main distribution ex-

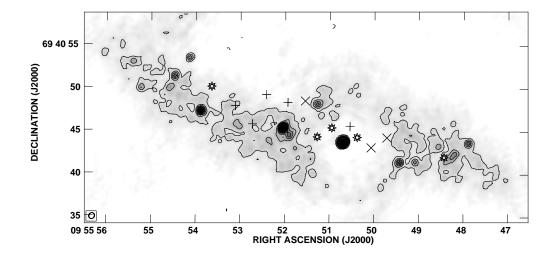


Figure 9. Positions of the masers plotted over the $408\,\mathrm{MHz}$ emission from MERLIN observations in 1994 from Wills et al. (1997). Contours are plotted at (-2, 2, 4, 6, 8, 10, 12, 14, 16, 18, 20) \times 1 mJy/bm. As for Figure 7, masers visible at just 1665 MHz, just 1667 MHz, or both, are shown by plus, cross and star symbols repectively. The masers avoid the areas of emission with the brightest masers sited in the extended absorption region surrounding the source 41.95+57.5, see Section 6.3.

pected for a rotating disk. With the exception of 50.54+45.5, all of these masers are weaker at $1665\,\mathrm{MHz}.$

50.54+45.5 is the odd one out in this group since, despite appearing to be part of the group spatially, dynamically it is quite separate. Velocity measurements clearly place it not in the blue arc on the p-v diagram but on the main disk distribution tracing the bulk rotation of the galaxy. It is also the only maser in this group which is visible only at $1665 \, \text{MHz}$, giving it a line ratio of $<1 \, \text{and}$, of the masers in this group, $50.54+45.5 \, \text{lies}$ closest to the edge of the dust lane in the optical map.

These observations confirm the results from Argo et al. (2007) that the brightest masers exist on this blue ward feature. As well as being clustered in frequency, they are clustered spatially, in an apparent arc to the north of the strong continuum source 41.95+57.5. Comparing the positions of the masers with optical emission in Figure 7, the masers in this group are located in a thick dust lane to the South of a bright knot. They are also all spatially located around the [NeII] features W1 and W2 from Achtermann & Lacy (1995) which shows a similar velocity distribution to that of the masers.

7 CONCLUSIONS

Sensitive, high spectral resolution observations of the M82 starburst have been carried out at 1.6 GHz using the VLA in A-configuration. The observations confirm previous detections and discovered three previously undetected masers. All the masers are significantly brighter than typical Galactic masers, an effect which is probably due to the superposition of several masing clouds along a particular line of sight, a conclusion supported by the velocity structure we are starting to see in these higher resolution observations.

The spatial distribution of the masers follows that of the continuum emission with most of the masers apparently coincident with continuum objects and/or other maser species. Their distribution in p-v space largely follows that of the absorption seen in HI. Most of the masers are located on the main velocity distribution which traces the bulk motion in the disk, however three of the brightest masers are located on a significant blue ward feature around a 'hole' observed previously in HI and CO, and traced particularly well by [Neil] emission. If this group of masers is tracing out an inner ring, as suggested by comparisons with the [NeII] emission, then it might be expected that a corresponding group would be seen on the eastern side of the dynamical centre with redshifted velocities compared to the bulk distribution. Such a feature is not traced either by maser emission or OH absorption, although a hint of such a structure was noted in HI by Wills et al. (2000).

Despite the improvement over previous observations, many of the masers are still largely unresolved in frequency. However, those on the blue ward feature do show some interesting structures with multiple velocity components, supporting the idea that several maser features are being detected along one line of sight. This structure is apparent at both 1665 and 1667 MHz with all three masers more extended on the p-v diagram at 1667 MHz. 50.95+45.4 shows particularly interesting structure with evidence of multiple components both spatially and in velocity.

Acknowledgements

The VLA is operated by the National Radio Astronomy Observatory, a facility of the National Science Foundation operated under cooperative agreement by Associated Universities, Inc. This research has made use of software provided by the UK's AstroGrid Virtual Observatory Project, which

is funded by the Science and Technology Facilities Council and through the EU's Framework 6 programme. RJB acknowledges support from the European Commission's I3 programme "RADIONET" under contract 505818.

REFERENCES

- Achtermann J. M., Lacy J. H., 1995, Astrophys. J., 439, 163
- Argo M. K., Pedlar A. P., Beswick R. J., Muxlow T. W. B. M., 2007, MNRAS, 380, 596
- Baudry A., Brouillet N., 1996, Astron. Astrophys., 316, 188 Beirão P., Brandl B. R., Appleton P. N., Groves B., Armus L., Förster Schreiber N. M., Smith J. D., Charmandaris V., Houck J. R., 2008, Astrophys. J., 676, 304
- Fenech D. M., Muxlow T. W. B., Beswick R. J., Pedlar A., Argo M. K., 2008, Mon. Not. R. Astr. Soc., 391, 1384
- Freedman W. L., Hughes S. M., Madore B. F., Mould J. R., Lee M. G., Stetson P., Kennicutt R. C., Turner A., Ferrarese L., Ford H., Graham J. A., Hill R., Hoessel J. G., Huchra J., Illingworth G. D., 1994, Astrophys. J., 427, 628
- Griffiths R. E., Ptak A., Feigelson E. D., Garmire G., Townsley L., Brandt W. N., Sambruna R., Bregman J. N., 2000, Science, 290, 1325
- Impellizzeri C. M. V., McKean J. P., Castangia P., Roy A. L., Henkel C., Brunthaler A., Wucknitz O., 2008, Nature, 456, 927
- Lo K. Y., 2005, Ann. Rev. Astron. Astrophys., 43, 625
- Lonsdale C. J., 2002, in IAU Symposium, Vol. 206, Cosmic Masers: From Proto-Stars to Black Holes, Migenes V., Reid M. J., eds., pp. 413-+
- Matsushita S., Kawabe R., Kohno K., Matsumoto H., Tsuru T. G., Vila-Vilaró B., 2005, Astrophys. J., 618, 712
- McDonald A. R., Muxlow T. W. B., Wills K. A., Pedlar A., Beswick R. J., 2002, Mon. Not. R. Astr. Soc., 334, 912
- Muxlow T. W. B., Pedlar A., Wilkinson P. N., Axon D. J., Sanders E. M., de Bruyn A. G., 1994, Mon. Not. R. Astr. Soc., 266, 455
- Rodriguez-Rico C. A., Viallefond F., Zhao J.-H., Goss W. M., Anantharamaiah K. R., 2004, Astrophys. J., 616, 783
- Seaquist E. R., Frayer D. T., Frail D. A., 1997, Astrophys. J., 487, L131
- Seaquist E. R., Lee S. W., Moriarty-Schieven G. H., 2006, Astrophys. J., 638, 148
- Shen J., Lo K. Y., 1995, Astrophys. J. Letters, 445, L99
- Shopbell P. L., Bland-Hawthorn J., 1998, Astrophys. J., 493, 129
- Weliachew L., Fomalont E. B., Greisen E. W., 1984, Astron. Astrophys., 137, 355
- Westmoquette M. S., Smith L. J., Gallagher J. S., Trancho G., Bastian N., Konstantopoulos I. S., 2009, Astrophys. J., 696, 192
- Wills K. A., Das M., Pedlar A., Muxlow T. W. B., Robinson T. G., 2000, Mon. Not. R. Astr. Soc., 316, 33
- Wills K. A., Pedlar A., Muxlow T. W. B., Stevens I. R., 1999, Mon. Not. R. Astr. Soc., 305, 680
- Wills K. A., Pedlar A., Muxlow T. W. B., Wilkinson P. N., 1997, Mon. Not. R. Astr. Soc., 291, 517